Available online at www.sciencedirect.com

ScienceDirect

Advances in Space Research xxx (xxxx) xxx

ADVANCES IN SPACE RESEARCH (a COSPAR publication)

www.elsevier.com/locate/asr

Design and analysis of attitude observers based on the Lagrange-d'Alembert principle applied to constrained three-vehicle formations

Pedro Cruz [a,*], Pedro Batista [a], Amit Sanyal [b]

[a] Institute for Systems and Robotics, Laboratory for Robotics and Engineering Systems, Instituto Superior Técnico, Universidade de Lisboa, Portugal
[b] Department of Mechanical & Aerospace Engineering of the College of Engineering and Computer Science at Syracuse University, Syracuse, NY, United States

Received 7 July 2021; received in revised form 20 January 2022; accepted 7 March 2022

Abstract

Constrained formations of vehicles are interesting in a variety of space mission scenarios for their potential ability to solve complex problems with relatively simple and specialized individual systems. However, the analysis of such formations can present some challenges. In this paper, an attitude observer is designed with the intent of applying it to three-vehicle heterogeneous formations with no line of sight between two of the vehicles. Each vehicle measures directions to other vehicles and independent inertial reference vectors. The relative direction between the two vehicles with no line of sight cannot be measured. Under some assumptions, these relative measurements yield a reconstructed attitude, which, together with the angular velocities measured by rate gyros, drive the observers. The attitude observers are identical and independently applied to each vehicle. Their design is based on the Lagrange-d'Alembert principle of variational mechanics, considering only kinematic models. The attitude observers are locally exponentially stable and each estimation error is shown to converge to zero error for almost all initial conditions. Finally, a series of numerical Monte Carlo simulations of the discrete-time form of the observers validate the stability and convergence characteristics of the observers under the appropriate assumptions on the availability of a reconstructed attitude.

Keywords: Attitude Estimation; Spacecraft Formation; Constrained Formation; Lagrange-D'Alembert Principle; Attitude Measurement

1. Introduction

Formations are appealing to many scientific fields because they can accomplish complex missions with relatively simple individual systems, which are inherently easier to build and deploy (Cao et al., 1997). In the spaceflight context, a formation should be distinguished from a constellation, because there is a coupling between the dynamic states of its elements (Scharf et al., 2003).

The constrained formation considered in this paper was studied in (Cruz and Batista, 2019), where the measurement of some vehicles is restricted, either by the sensor capacity or by environment imposed limitations. An attitude estimation problem for a three-vehicle formation can be found in (Andrle et al., 2009) and an application to that problem is found in (Wang et al., 2019), which considers a formation of small satellites. An extended Kalman filter is applied to the three-vehicle formation in (Kim et al., 2007) using rate-gyros to measure the angular velocity. In (Linares et al., 2011), the attitude of a two vehicle constrained formation with a common landmark is deter-

* Corresponding author.
E-mail addresses: pfcruz@isr.tecnico.ulisboa.pt (P. Cruz), pbatista@isr.tecnico.ulisboa.pt (P. Batista), aksanyal@syr.edu (A. Sanyal).

https://doi.org/10.1016/j.asr.2022.03.003
0273-1177/

mined. More recently, (Wu, 2020) considered an attitude problem where both hand-eye and vector measurements were used to minimize a cost function and determine the relative attitude between two spacecraft.

Such systems find some of its applications in the context of space missions, more specifically if the distance between the elements of the formation is large. Examples can be found, for instance, when synthesizing large aperture telescopes or long baseline interferometers far from Earth, or even when sampling spatially disperse phenomena such as the Earth's magnetotail (Cesarone et al., 2007).

An important problem in many space systems is that of attitude estimation, that is, the knowledge of the relative orientation between two relevant coordinate frames. Early attitude estimation methods include deterministic approaches such as the Tri-Axial Attitude Determination (TRIAD) algorithm (Black, 1964) and solutions of the Wahba's problem (Wahba, 1965). Examples for the latter and other nonlinear estimation methods can be found in (Crassidis et al., 2007). The design of an estimation method considers different goals. Some methods seek fast or even optimal performance (Wu et al., 2018), some look for robustness (Sanyal et al., 2008), while others prioritize low computational complexity for cost reduction. Often, a combination of these and other goals are considered (Batista et al., 2012).

A useful strategy to design filtering schemes is using the minimization of an "energy" function, which can be helpful in fulfilling stability criteria. These can be implemented using the Hamilton–Jacobi-Bellman theory (Aguiar and Hespanha, 2006; Zamani et al., 2011), but also by applying the variational mechanics principles (Izadi and Sanyal, 2014). These principles have been applied not only to spacecraft (Misra et al., 2016), but also to landing rovers (Li et al., 2020).

This work follows those same principles to obtain an estimate for all the attitudes of the three vehicle constrained formation proposed in (Cruz and Batista, 2019), while accounting for the attitude kinematics and with stability assurances. The purpose of designing such an observer is to improve the accuracy of the estimate by filtering the measurement noise using angular velocity information, which won't be the case if the attitude determination was carried out at every time instant that measurements were obtained. Additionally, sensors that measure angular velocity values are common in spacecraft. Therefore, since attitude observers can be driven by reconstructed attitudes (Mahony et al., 2008) and there is an appropriate deterministic algorithm for attitude reconstruction in this formation, the observer in this paper is driven by such variables, instead of being directly driven by the measurements.

The main contribution of this paper is the design of an attitude observer which filters the errors of the deterministic attitude reconstruction by considering angular velocity measurements. Furthermore, the design of attitude filters for formations has not been extensively developed, and thus, attitude filters for constrained formations of vehicles are not that common in the literature. Previous work by the authors can be found in (Cruz et al., 2021). This paper presents a unified and thorough presentation and analysis of the solution, and it includes all the theorems and proofs that had been omitted in the conference paper. Finally, extensive and realistic simulations are also presented in detail, including the performance evaluation with Monte Carlo runs.

This paper is organized as follows. Section II describes the constrained formation, the attitude estimation problem, and the attitude reconstruction algorithm. In Section III, the observer is derived based on variational mechanics. This method relies on an energy-like function of the estimation errors, which is given by the Lagrangian and the application of the Lagrange-d'Alembert principle. The stability analysis follows and it is shown that the observer error converges to zero for almost all initial conditions and also that the origin is locally exponentially stable. Next, a first order discrete-time implementation of the filter is summarized in Section IV, which is derived from the discrete-time Lagrange-d'Alembert principle (Marsden and West, 2001). Finally, in Section V, the discrete-time filter is implemented in numerical simulations, which in a series of Monte Carlo runs evidence the convergence characteristics and performance of the observer.

2. Problem statement

2.1. Notation

Throughout this document, scalars are expressed in regular typeface and regular case, vectors are expressed in bold and regular case, and matrices are expressed in bold and upper case. The symbol $\mathbf{0}$ represents the null vector or matrix and $\mathbf{I}$ represents the identity matrix. The set of unit vectors in $\mathbb{R}^3$ is denoted by $\mathbb{S}^2 := \{\mathbf{x} \in \mathbb{R}^3 : \|\mathbf{x}\| = 1\}$. The special orthogonal group of dimension 3, which describes proper rotations, is denoted by

$$\mathrm{SO}(3) := \{\mathbf{X} \in \mathbb{R}^{3\times 3} : \mathbf{X}\mathbf{X}^{\mathrm{T}} = \mathbf{X}^{\mathrm{T}}\mathbf{X} = \mathbf{I} \wedge \det(\mathbf{X}) = 1\}.$$

The skew-symmetric matrix parameterized by $\mathbf{x} \in \mathbb{R}^3$, which encodes the cross product operator in $\mathbb{R}^3$, is denoted by

$$\mathbf{S}(\mathbf{x}) := \begin{bmatrix} 0 & -x_3 & x_2 \\ x_3 & 0 & -x_1 \\ -x_2 & x_1 & 0 \end{bmatrix},$$

with $\mathbf{x} = [x_1\, x_2\, x_3]^{\mathrm{T}}$. Therefore, $\mathbf{S}(\mathbf{x})\mathbf{y} = \mathbf{x} \times \mathbf{y}$, with $\mathbf{y} \in \mathbb{R}^3$, and $\mathbf{S}^{-1}(.)$ denotes the unskew operator, i.e. $\mathbf{S}^{-1}(\mathbf{S}(\mathbf{x})) = \mathbf{x}$.

The rotation matrix in SO(3) that transforms a given vector, in $\mathbb{R}^3$, expressed in the body-fixed frame of vehicle j into the inertial frame is denoted by $\mathbf{R}_j^I$. If the rotation transforms a vector from the body-fixed frame of the j-th vehicle to the body-fixed frame of the i-th vehicle it is rep-

resented as $\mathbf{R}_j^i$, instead. The rotation matrix of an angle $\theta \in \mathbb{R}$ about the axis described by the unit vector $\mathbf{x} \in \mathbb{S}^2$ is denoted by $\mathbf{R}(\theta, \mathbf{x})$, which is written as (Markley and Crassidis, 2014)

$$\mathbf{R}(\theta, \mathbf{x}) := \cos(\theta)\mathbf{I} + (1 - \cos(\theta))\mathbf{x}\mathbf{x}^{\mathrm{T}} - \sin(\theta)\mathbf{S}(\mathbf{x}). \quad (1)$$

Finally, the four-quadrant inverse tangent function is denoted by $\operatorname{atan2}(b, a)$, with $a, b \in \mathbb{R}$, and the inverse cosine function is denoted as $\arccos(a)$.

2.2. Problem statement

Consider a formation with three vehicles, each with a body-fixed coordinate frame. All vehicles are equipped with vision-based sensors, which measure directions with respect to other vehicles in their lines of sight, and sensors that measure directions of inertial references, such as the direction to a cluster of stars, a magnetic field, or other known references. Finally, it is assumed that each vehicle has three orthogonally-mounted rate gyros, which give a measurement of the angular velocity vector. Each sensor gives measurements in their respective body-fixed coordinate frames.

The measurement set of each element of the formation comprises its own angular velocity, one reference direction, and directions to at least one vehicle. The deputies, which is the designation of vehicles 2 and 3, cannot measure the relative direction with respect to one another, because the line of sight between them is assumed limited. In contrast, vehicle 1 measures relative directions to both deputies. The formation and respective measurements are depicted in Fig. 1.

The letter $\mathbf{d}$ denotes the direction measurements, while the symbol $\boldsymbol{\omega}$ denotes the angular velocity measurements. The subscript in the reference direction and angular velocity measurements indicates the vehicle taking the measurement, whereas the subscript in the relative measurements indicates both the vehicle taking the measurement and the respective target, i.e., the subscript j/k indicates that the measurement was taken by vehicle j and it is a relative direction pointing to vehicle k. Moreover, a left superscript indicates the frame where the measurement is represented, for instance, ${}^I\mathbf{d}_j$ is the measurement taken by vehicle j represented in the inertial frame. The left superscript is omitted if the frame in which the vector is represented coincides with the body-fixed frame of the vehicle taking the measurement. Therefore, the four relative measurements are denoted as $\mathbf{d}_{1/2}, \mathbf{d}_{2/1}, \mathbf{d}_{1/3}$, and $\mathbf{d}_{3/1}$, the measurements of the inertial references are denoted as $\mathbf{d}_1, \mathbf{d}_2$, and $\mathbf{d}_3$, which, in the inertial frame, are respectively denoted as ${}^I\mathbf{d}_1, {}^I\mathbf{d}_2$, and ${}^I\mathbf{d}_3$. The value of the latter is assumed to be known. Finally, the angular velocity of each vehicle is respectively represented as $\boldsymbol{\omega}_1, \boldsymbol{\omega}_2$, and $\boldsymbol{\omega}_3$. These are assumed to be continuous, bounded, and unbiased.

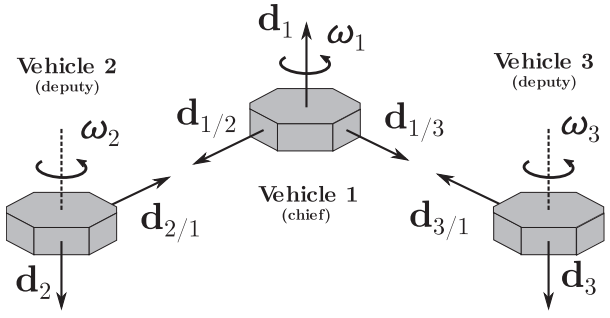

Fig. 1. Three-vehicle heterogeneous formation.

The attitude kinematics of the j-th vehicle is given by

$$\dot{\mathbf{R}}_j^I(t) = \mathbf{R}_j^I(t)\mathbf{S}\big(\boldsymbol{\omega}_j(t)\big). \quad (2)$$

The observer kinematics is a copy of the true attitude kinematics, which with the observer internal representation of the attitude and angular velocity denoted by $\hat{\boldsymbol{\omega}}_j$, is given, for vehicle j, as

$$\dot{\hat{\mathbf{R}}}_j^I(t) = \hat{\mathbf{R}}_j^I(t)\mathbf{S}\big(\hat{\boldsymbol{\omega}}_j(t)\big). \quad (3)$$

The problem addressed in this paper is the design of attitude estimators for $\big(\mathbf{R}_1^I, \mathbf{R}_2^I, \mathbf{R}_3^I\big)$. Moreover, their respective errors must converge to zero for almost all initial conditions. The estimates of the relative attitudes, $\big(\mathbf{R}_2^1, \mathbf{R}_3^1, \mathbf{R}_3^2\big)$, result from the inertial set, because these are defined by $\mathbf{R}_2^1 = (\hat{\mathbf{R}}_j^I)^{\mathrm{T}}\mathbf{R}_2^I$, $\mathbf{R}_3^1 = (\hat{\mathbf{R}}_j^I)^{\mathrm{T}}\mathbf{R}_3^I$, and $\mathbf{R}_3^2 = \hat{\mathbf{R}}_2^{I\,\mathrm{T}}\mathbf{R}_3^I$, respectively.

2.3. Attitude Reconstruction

The direction vector measurements and the inertial references can be used to reconstruct both relative and inertial attitudes of the formation by applying the deterministic algorithm in (Cruz and Batista, 2019). The observers proposed in the sequel are driven by such reconstructed inertial attitudes. Since this algorithm is employed in the simulation section, it is summarized here for the sake of completeness.

The basic idea is to use the formation symmetries to obtain a set of candidates for the inertial attitude of the chief. Then, comparing such candidates, one can find the correct attitudes, because they must be consistent regardless of the variables used in their construction. Consider the problem geometric constraint given as $-\mathbf{d}_{1/2} = \mathbf{R}_2^1\mathbf{d}_{2/1}$ and define

$$\mathbf{x}_1 := \begin{cases} \frac{\mathbf{d}_{2/1} - \mathbf{d}_{1/2}}{\left\|\mathbf{d}_{2/1} - \mathbf{d}_{1/2}\right\|} & , \text{if } \mathbf{d}_{2/1} \neq \mathbf{d}_{1/2} \\ \frac{\mathbf{S}(\mathbf{d}_1)\mathbf{d}_{1/2}}{\left\|\mathbf{S}(\mathbf{d}_1)\mathbf{d}_{1/2}\right\|} & , \text{if } \mathbf{d}_{2/1} = \mathbf{d}_{1/2} \end{cases}.$$

It follows that $-\mathbf{d}_{1/2} = \mathbf{R}\big(\theta_2, -\mathbf{d}_{1/2}\big)\mathbf{R}(\pi, \mathbf{x}_1)\mathbf{d}_{2/1}$ for any $\theta_2 \in \mathbb{R}$. Hence, consider that

$$\mathbf{R}_2^1 = \mathbf{R}\big(\theta_2, -\mathbf{d}_{1/2}\big)\mathbf{R}(\pi, \mathbf{x}_1). \quad (4)$$

Then, the result of substituting (4) in the geometric constraint given by ${}^I\mathbf{d}_1^{\mathrm{T}I}\mathbf{d}_2 = \mathbf{d}_1^{\mathrm{T}}\mathbf{R}_2^1\mathbf{d}_2$ can be expressed as (Cruz and Batista, 2019)

$$a_{p_{12}} = a_{c_{12}}\cos(\theta_2) + a_{s_{12}}\sin(\theta_2), \quad (5)$$

where $a_{s_{12}}, a_{c_{12}}$, and $a_{p_{12}}$ are scalar coefficients, which are associated with the trigonometric constraints of the relation between vehicles 1 and 2. The value of such coefficients are given by

$$a_{s_{12}} := \mathbf{d}_1^{\mathrm{T}}\mathbf{S}(-\mathbf{d}_{1/2})\mathbf{R}(\pi, \mathbf{x}_1)\mathbf{d}_2,$$
$$a_{c_{12}} := \mathbf{d}_1^{\mathrm{T}}\mathbf{S}(\mathbf{d}_{1/2})^2\mathbf{R}(\pi, \mathbf{x}_1)\mathbf{d}_2,$$
and
$$a_{p_{12}} := \mathbf{d}_1^{\mathrm{T}}\mathbf{d}_{1/2}\mathbf{d}_{1/2}^{\mathrm{T}}\mathbf{R}(\pi, \mathbf{x}_1)\mathbf{d}_2 - {}^I\mathbf{d}_1^{\mathrm{T}}{}^I\mathbf{d}_2.$$

Solving the trigonometric equation in (5) results in

$$\theta_2 := \operatorname{atan2}(a_{s_{12}}, a_{c_{12}}) \pm \arccos\left(\frac{a_{p_{12}}}{\sqrt{a_{s_{12}}^2 + a_{c_{12}}^2}}\right). \tag{6}$$

Since different candidates result from the different signs in (6), then the relative attitude candidate is given as

$$\left(\mathbf{R}_2^1\right)_X = \mathbf{R}(\theta_2, -\mathbf{d}_{1/2})\mathbf{R}(\pi, \mathbf{x}_1),$$

where X identifies the respective candidate. If $\mathbf{d}_1$ is transverse to $\left(\mathbf{R}_2^1\right)_X\mathbf{d}_2$, then the respective inertial candidate results from the TRIAD algorithm and is given by

$$\left(\mathbf{R}_1^I\right)_X := {}^I\mathbf{d}_1\mathbf{d}_1^{\mathrm{T}} + \frac{\mathbf{S}({}^I\mathbf{d}_1){}^I\mathbf{d}_2\left[\mathbf{S}(\mathbf{d}_1)\left(\mathbf{R}_2^1\right)_X\mathbf{d}_2\right]^{\mathrm{T}}}{\|\mathbf{S}({}^I\mathbf{d}_1){}^I\mathbf{d}_2\|\left\|\mathbf{S}(\mathbf{d}_1)\left(\mathbf{R}_2^1\right)_X\mathbf{d}_2\right\|} + \frac{\mathbf{S}({}^I\mathbf{d}_1)\mathbf{S}({}^I\mathbf{d}_1){}^I\mathbf{d}_2\left[\mathbf{S}(\mathbf{d}_1)\mathbf{S}(\mathbf{d}_1)\left(\mathbf{R}_2^1\right)_X\mathbf{d}_2\right]^{\mathrm{T}}}{\|\mathbf{S}({}^I\mathbf{d}_1){}^I\mathbf{d}_2\|\left\|\mathbf{S}(\mathbf{d}_1)\left(\mathbf{R}_2^1\right)_X\mathbf{d}_2\right\|}.$$

The analogous relative candidate is obtained by considering the analogous parameterization of $\mathbf{R}_3^1$ and the analogous parameters $\mathbf{x}_3$ and θ_4. Hence, it is given as

$$\left(\mathbf{R}_3^1\right)_Y = \mathbf{R}(\theta_4, -\mathbf{d}_{1/3})\mathbf{R}(\pi, \mathbf{x}_3).$$

Again, the respective inertial candidate $\left(\mathbf{R}_1^I\right)_Y$ results from the TRIAD algorithm, but with the measurement pairs $({}^I\mathbf{d}_1, \mathbf{d}_1)$ and $\left({}^I\mathbf{d}_3, \left(\mathbf{R}_3^1\right)_Y\mathbf{d}_3\right)$ instead.

From the comparison between the four candidates for $\mathbf{R}_1^I$, the correct attitude is given by finding identical candidates, i.e., the candidate pair which results in the lowest value of a metric given by

$$\mu = \left|\arccos\left(\frac{\operatorname{trace}\left(\left(\mathbf{R}_1^I\right)_X^{\mathrm{T}}\left(\mathbf{R}_1^I\right)_Y\right) - 1}{2}\right)\right|.$$

By construction and in the absence of noise, the solution yields $\mu = 0$, so $\left(\mathbf{R}_1^I\right)_X$ should be equal to $\left(\mathbf{R}_1^I\right)_Y$. In the presence of noise, the pair with the lowest μ is selected and averaged.

Finally, once the solutions for $\mathbf{R}_1^I, \mathbf{R}_2^1$, and $\mathbf{R}_3^1$ are available, the solutions for $\mathbf{R}_2^I$ and $\mathbf{R}_3^I$ follow immediately from $\mathbf{R}_2^I = \mathbf{R}_1^I\mathbf{R}_2^1$ and $\mathbf{R}_3^I = \mathbf{R}_1^I\mathbf{R}_3^1$.

In general, there is a unique solution. Nonetheless, in specific configurations, there may be multiple solutions. Thus, in the simulations, it is assumed that the configuration is such that the deterministic algorithm gives a unique solution, see (Cruz and Batista, 2020) for the characterization of the conditions of the solution.

3. Observer Design

The ensuing attitude observer results directly from the application of the Lagrange-d'Alembert principle of variational mechanics. It assumes that the inertial attitudes reconstructed from the measurement set are available, which can be accomplished with the algorithm described in the previous section. Since the three observers are identical and driven by analogous variables, then a single vehicle is considered throughout this section.

First, a Lagrangian function is constructed to represent an energy-like function of the estimation errors. Then, the Lagrange-d'Alembert principle applied to the sum of the first variation of the action functional and a dissipation term gives the dynamics of the observer feedback term. For readability, the time dependence of the variables is omitted in this section.

3.1. Lagrangian

Consider the j-th vehicle of the formation. Its observer internal representation of the angular velocity is given by the difference between the true angular velocity and a feedback term, $\boldsymbol{\phi}_j$, as follows

$$\hat{\boldsymbol{\omega}}_j = \boldsymbol{\omega}_j - \boldsymbol{\phi}_j. \tag{7}$$

The associated kinetic energy-like function is defined as

$$T_j := \frac{m_j}{2}\left(\boldsymbol{\omega}_j - \hat{\boldsymbol{\omega}}_j\right)^{\mathrm{T}}\left(\boldsymbol{\omega}_j - \hat{\boldsymbol{\omega}}_j\right) = \frac{m_j}{2}\boldsymbol{\phi}_j^{\mathrm{T}}\boldsymbol{\phi}_j,$$

where m_j is a positive weight constant. The inertial attitude error matrix of vehicle j is given by

$$\mathbf{Q}_j^I = \mathbf{R}_j^I(\hat{\mathbf{R}}_j^I)^{\mathrm{T}}. \tag{8}$$

The associated potential energy-like function is defined as

$$U_j := p_j\operatorname{trace}\left(\mathbf{I} - \mathbf{Q}_j^I\right),$$

where p_j is a positive weight constant. Finally, the Lagrangian of the formation is given by

$$\mathscr{L}_j = T_j - U_j = \frac{m_j}{2}\boldsymbol{\phi}_j^{\mathrm{T}}\boldsymbol{\phi}_j - p_j\operatorname{trace}\left(\mathbf{I} - \mathbf{Q}_j^I\right).$$

3.2. First variation of the action functional

The action functional is defined as the time integral of the Lagrangian function. Thus, its first variation is given by

$$\delta s_j = \int_{t_0}^{t_f}\delta\mathscr{L}_j\,dt = \int_{t_0}^{t_f}\delta T_j - \delta U_j\,dt, \tag{9}$$

where t_0 and t_f are the initial and final time of estimation, respectively. The estimated inertial attitude first variation of the j-th vehicle is given as $\delta\hat{\mathbf{R}}_j^I = \hat{\mathbf{R}}_j^I\mathbf{S}(\eta_j)$, where η_j is a

perturbation function. Moreover, from the attitude kinematics, the first variation of the observer internal angular velocity is given by $\delta\hat{\boldsymbol{\omega}}_j = \dot{\eta}_j + \mathbf{S}(\hat{\boldsymbol{\omega}}_j)\eta_j$, see (Izadi and Sanyal, 2014). Therefore, the first variation of the kinematic term is expressed as

$$\delta T_j = -m_j(\boldsymbol{\omega}_j - \hat{\boldsymbol{\omega}}_j)^{\mathrm{T}}(\dot{\eta}_j + \mathbf{S}(\hat{\boldsymbol{\omega}}_j)\eta_j),$$

or, equivalently,

$$\delta T_j = -m_j\boldsymbol{\phi}_j^{\mathrm{T}}(\dot{\eta}_j + \mathbf{S}(\hat{\boldsymbol{\omega}}_j)\eta_j). \tag{10}$$

The first variation of the potential term is given by

$$\delta U_j = p_j \mathrm{trace}\Big(\mathbf{R}_j^I(\hat{\mathbf{R}}_j^I)^{\mathrm{T}}\mathbf{S}(\eta_j)\Big),$$

which, decomposing $\mathbf{R}_j^I\hat{\mathbf{R}}_j^{I\mathrm{T}}$ into

$$\mathbf{R}_j^I(\hat{\mathbf{R}}_j^I)^{\mathrm{T}} = \frac{1}{2}\Big(\mathbf{R}_j^I(\hat{\mathbf{R}}_j^I)^{\mathrm{T}} + \hat{\mathbf{R}}_j^I(\hat{\mathbf{R}}_j^I)^{\mathrm{T}}\Big) + \frac{1}{2}\Big(\mathbf{R}_j^I(\hat{\mathbf{R}}_j^I)^{\mathrm{T}} - \hat{\mathbf{R}}_j^I(\hat{\mathbf{R}}_j^I)^{\mathrm{T}}\Big)$$

and noticing that the trace of the product between a symmetric and skew symmetric matrix is zero, gives

$$\delta U_j = p_j \mathrm{trace}\left(\frac{1}{2}\Big(\mathbf{R}_j^I(\hat{\mathbf{R}}_j^I)^{\mathrm{T}} - \hat{\mathbf{R}}_j^I(\hat{\mathbf{R}}_j^I)^{\mathrm{T}}\Big)\mathbf{S}(\eta_j)\right).$$

Lastly, from $\mathrm{trace}(\mathbf{S}(\mathbf{a})\mathbf{S}(\mathbf{b})) = -2\mathbf{a}^{\mathrm{T}}\mathbf{b}$ with $\mathbf{a}, \mathbf{b} \in \mathbb{R}^3$, it follows that

$$\delta U_j = -p_j\mathbf{S}^{-1}\Big(\mathbf{R}_j^I(\hat{\mathbf{R}}_j^I)^{\mathrm{T}} - \hat{\mathbf{R}}_j^I(\hat{\mathbf{R}}_j^I)^{\mathrm{T}}\Big)^{\mathrm{T}}\eta_j. \tag{11}$$

3.3. Observer feedback dynamics

Consider a positive definite matrix $\mathbf{D}_j$ and define a dissipation term as $\tau_j^{\mathrm{T}}\eta_j = \boldsymbol{\phi}_j^{\mathrm{T}}\mathbf{D}_j\eta_j$. Then, applying the Lagrange-d'Alembert principle to the sum of the action functional and dissipation, i.e. $\delta s_j + \int_{t_0}^{t_f}\tau_j^{\mathrm{T}}\eta_j\,dt = 0$, and recalling (9)-(11), yields

$$\int_{t_0}^{t_f}\Big\{-m_j\boldsymbol{\phi}_j^{\mathrm{T}}\dot{\eta}_j - m_j\boldsymbol{\phi}_j^{\mathrm{T}}\mathbf{S}(\hat{\omega}_j)\eta_j + p_j\mathbf{S}^{-1}(\mathbf{M}_j)^{\mathrm{T}}\eta_j + (\mathbf{D}_j\boldsymbol{\phi}_j)^{\mathrm{T}}\eta_j\Big\}dt = 0,$$

where $\mathbf{M}_j := (\hat{\mathbf{R}}_j^I)^{\mathrm{T}}\mathbf{R}_j^I - (\hat{\mathbf{R}}_j^I)^{\mathrm{T}}\hat{\mathbf{R}}_j^I$. Since the perturbation function is zero at t_0 and at t_f, then integrating the first term by parts gives

$$\int_{t_0}^{t_f}\Big\{\big[m_j\dot{\boldsymbol{\phi}}_j + (m_j\mathbf{S}(\hat{\boldsymbol{\omega}}_j) + \mathbf{D}_j)\boldsymbol{\phi}_j + p_j\mathbf{S}^{-1}(\mathbf{M}_j)\big]^{\mathrm{T}}\eta_j\Big\}dt = 0.$$

Finally, the fundamental lemma of the calculus of variations, yields an equation which encodes the estimator feedback term dynamics. Thus, the observer equations are given as

$$\dot{\hat{\mathbf{R}}}_j^I = \hat{\mathbf{R}}_j^I\mathbf{S}(\hat{\boldsymbol{\omega}}_j) \tag{12a}$$

and

$$m_j\dot{\boldsymbol{\phi}}_j = -(m_j\mathbf{S}(\hat{\boldsymbol{\omega}}_j) + \mathbf{D}_j)\boldsymbol{\phi}_j - p_j\mathbf{S}^{-1}(\mathbf{M}_j). \tag{12b}$$

3.4. Observer stability

The error dynamics are studied under the assumption that the measurements are free of noise. In such conditions, the error is shown to converge asymptotically to zero for almost all initial configurations. Furthermore, the origin is locally exponentially stable. The attitude observer performance in the presence of sensor noise is assessed in the simulation section.

Take the time derivative of (8) and expand using (2) and (3). Recalling (7), it follows that

$$\dot{\mathbf{Q}}_j^I = \mathbf{R}_j^I\mathbf{S}(\boldsymbol{\omega}_j)\hat{\mathbf{R}}_j^{I\mathrm{T}} + \mathbf{R}_j^I\mathbf{S}(\hat{\boldsymbol{\omega}}_j)^{\mathrm{T}}\hat{\mathbf{R}}_j^{I\mathrm{T}} = \mathbf{R}_j^I\mathbf{S}(\boldsymbol{\phi}_j)\hat{\mathbf{R}}_j^{I\mathrm{T}}.$$

or, equivalently, $\dot{\mathbf{Q}}_j^I = \mathbf{S}\Big(\mathbf{R}_j^I\boldsymbol{\phi}_j\Big)\mathbf{Q}_j^I$. The observer feedback dynamics remain the same as in (12b), although their dependence on $\mathbf{Q}_j^I$ is evidenced by some rearrangements. Hence, the error system dynamics, considering the j-th vehicle, are given by

$$\dot{\mathbf{Q}}_j^I = \mathbf{S}\Big(\mathbf{R}_j^I\boldsymbol{\phi}_j\Big)\mathbf{Q}_j^I \tag{13a}$$

and

$$m_j\dot{\boldsymbol{\phi}}_j = -p_j\mathbf{S}^{-1}\Big((\hat{\mathbf{R}}_j^I)^{\mathrm{T}}[\mathbf{Q}_j^I - (\mathbf{Q}_j^I)^{\mathrm{T}}]\mathbf{R}_j^I\Big) - \Big[m_j\mathbf{S}(\hat{\boldsymbol{\omega}}_j) + \mathbf{D}_j^I\Big]\boldsymbol{\phi}_j. \tag{13b}$$

3.4.1. Equilibrium Points

The equilibrium points of the error system are found by substituting $\dot{\mathbf{Q}}_j^I = \mathbf{0}$ and $\dot{\boldsymbol{\phi}}_j = \mathbf{0}$ in (13), which yields

$$\mathbf{0} = \mathbf{S}\Big(\mathbf{R}_j^I\boldsymbol{\phi}_j\Big)\mathbf{Q}_j^I \tag{14a}$$

and

$$\mathbf{0} = -p_j\mathbf{S}^{-1}\Big((\hat{\mathbf{R}}_j^I)^{\mathrm{T}}\Big[\mathbf{Q}_j^I - (\mathbf{Q}_j^I)^{\mathrm{T}}\Big]\mathbf{R}_j^I\Big) - \Big[m_j\mathbf{S}(\hat{\boldsymbol{\omega}}_j) + \mathbf{D}_j^I\Big]\boldsymbol{\phi}_j. \tag{14b}$$

From (14a), $\boldsymbol{\phi}_j = \mathbf{0}$. Therefore, it follows that (14b) becomes

$$\mathbf{S}^{-1}\Big((\hat{\mathbf{R}}_j^I)^{\mathrm{T}}[\mathbf{Q}_j^I - (\mathbf{Q}_j^I)^{\mathrm{T}}]\mathbf{R}_j^I\Big) = \mathbf{0}$$

which implies that

$$\mathbf{Q}_j^I = (\mathbf{Q}_j^I)^{\mathrm{T}}, \tag{15}$$

which is satisfied by all attitude error matrices with an angle of 0° or 180°, considering their Euler axis/angle representation in (1). Hence, the error system is at the equilibrium when the feedback term is zero and the error matrix is symmetric.

Next, recall the Euler axis/angle parameterization, consider the axis and angle respectively given by $\mathbf{e} \in \mathbb{S}^2$ and $\epsilon \in \mathbb{R}$, and denote $\mathbf{Q}_j^I := \mathbf{R}(\epsilon, \mathbf{e})$. Then, rewrite (15) as

$$\mathbf{R}(\epsilon, \mathbf{e}) = [\mathbf{R}(\epsilon, \mathbf{e})]^{\mathrm{T}},$$

or, equivalently, $\mathbf{R}(2\epsilon, \mathbf{e}) = \mathbf{I}$. It follows, from (1) and the double angle trigonometric identities, that

$$\left[1 - \cos^2(\epsilon) + \sin^2(\epsilon)\right](\mathbf{e}\mathbf{e}^{\mathrm{T}} - \mathbf{I}) - 2\sin(\epsilon)\cos(\epsilon)\mathbf{S}(\mathbf{e}) = \mathbf{0}. \tag{16}$$

As consequence of the Pythagorean identity, *i.e.*

$$\sin^2(\epsilon) + \cos^2(\epsilon) = 1,$$

it is verified that $1 - \cos^2(\epsilon) + \sin^2(\epsilon) = 2\sin^2(\epsilon)$. Hence, applying such relation to (16), gives

$$2\sin(\epsilon)\sin(\epsilon)(\mathbf{e}\mathbf{e}^{\mathrm{T}} - \mathbf{I}) - 2\sin(\epsilon)\cos(\epsilon)\mathbf{S}(\mathbf{e}) = \mathbf{0}$$

or, equivalently,

$$\sin(\epsilon)\left[\sin(\epsilon)(\mathbf{e}\mathbf{e}^{\mathrm{T}} - \mathbf{I}) - \cos(\epsilon)\mathbf{S}(\mathbf{e})\right] = \mathbf{0}. \tag{17}$$

If $\sin(\epsilon) = 0$, then $\epsilon = k\pi, k \in \mathbb{Z}$. Else, if $\sin(\epsilon) \neq 0$, then $\sin(\epsilon)(\mathbf{e}\mathbf{e}^{\mathrm{T}} - \mathbf{I}) = \cos(\epsilon)\mathbf{S}(\mathbf{e})$. However, the left hand side is symmetric, whereas the right hand side is skew symmetric, and both are different from zero, which means that this condition cannot be satisfied. Therefore, the solution for (17) is $\epsilon = k\pi, k \in \mathbb{Z}$.

The equilibrium points can be represented in a more compact form by recalling that $\mathrm{trace}\left(\mathbf{Q}_j^I\right) = 1 + 2\cos(\epsilon)$. Hence, for $\epsilon = 0 + 2k\pi, \mathrm{trace}\left(\mathbf{Q}_j^I\right) = 3$ and for $\epsilon = \pi + 2k\pi, \mathrm{trace}\left(\mathbf{Q}_j^I\right) = -1$. Then, define

$$S_j := \left\{\left(\mathbf{Q}_j^I, \boldsymbol{\phi}_j\right) | \mathrm{trace}\left(\mathbf{Q}_j^I\right) = 3, \boldsymbol{\phi}_j = \mathbf{0}\right\}, \tag{18}$$

which is the desired equilibrium point (zero estimation error). Define also the undesired equilibrium set as

$$U_j := \left\{\left(\mathbf{Q}_j^I, \boldsymbol{\phi}_j\right) | \mathrm{trace}\left(\mathbf{Q}_j^I\right) = -1, \boldsymbol{\phi}_j = \mathbf{0}\right\}. \tag{19}$$

The set of all equilibrium points is the union of both sets, which is denoted as $E_j = S_j \cup U_j$.

3.4.2. Observer stability

The following theorem details the stability characteristics of the observer.

Theorem 1. Consider the error system (13) and the equilibrium sets S_j and U_j, defined in (18) and (19), respectively. Assume that $\boldsymbol{\omega}_j$ is bounded. Then:

1. the set U_j is forward invariant and unstable relative to (13);
2. the set S_j is locally exponentially stable; and
3. the error converges to S_j for almost all initial conditions $\notin U_j$.

Proof. First, consider the Lyapunov candidate function given by

$$V(t) = \frac{m_j}{2}\boldsymbol{\phi}_j^{\mathrm{T}}\boldsymbol{\phi}_j + p_j\mathrm{trace}\left(\mathbf{I} - \mathbf{Q}_j^I\right), \tag{20}$$

whose time derivative is given as

$$\dot{V}(t) = \boldsymbol{\phi}_j^{\mathrm{T}}(m_j\dot{\boldsymbol{\phi}}_j) - p_j\mathrm{trace}\left(\dot{\mathbf{Q}}_j^I\right),$$

or, using (13), expressed as

$$\dot{V}(t) = \boldsymbol{\phi}_j^{\mathrm{T}}\left[-m_j\mathbf{S}(\hat{\boldsymbol{\omega}}_j)\boldsymbol{\phi}_j - p_j\mathbf{S}^{-1}(\mathbf{M}_j) - \mathbf{D}_j^I\boldsymbol{\phi}_j\right] - p_j\mathrm{trace}\left(\mathbf{R}_j^I\mathbf{S}(\boldsymbol{\phi}_j)(\hat{\mathbf{R}}_j^I)^{\mathrm{T}}\right). \tag{21}$$

Since $\boldsymbol{\phi}_j^{\mathrm{T}}\mathbf{S}(\hat{\boldsymbol{\omega}}_j)\boldsymbol{\phi}_j = 0$ and recalling the trace cyclic property, (21) is given as

$$\dot{V}(t) = -\boldsymbol{\phi}_j^{\mathrm{T}}p_j\mathbf{S}^{-1}(\mathbf{M}_j) - \boldsymbol{\phi}_j^{\mathrm{T}}\mathbf{D}_j^I\boldsymbol{\phi}_j - p_j\mathrm{trace}\left((\hat{\mathbf{R}}_j^I)^{\mathrm{T}}\mathbf{R}_j^I\mathbf{S}(\boldsymbol{\phi}_j)\right). \tag{22}$$

Then, recalling the procedure to obtain (11), rewrite (22) as

$$\dot{V}(t) = -p_j\boldsymbol{\phi}_j^{\mathrm{T}}\mathbf{S}^{-1}(\mathbf{M}_j) - \boldsymbol{\phi}_j^{\mathrm{T}}\mathbf{D}_j^I\boldsymbol{\phi}_j + p_j\boldsymbol{\phi}_j^{\mathrm{T}}\mathbf{S}^{-1}(\mathbf{M}_j).$$

Finally, $\dot{V}(t) = -\boldsymbol{\phi}_j^{\mathrm{T}}\mathbf{D}_j^I\boldsymbol{\phi}_j \leqslant 0$, which implies that $\boldsymbol{\phi}_j$ is bounded by the initial conditions of both $\boldsymbol{\phi}_j$ and $\mathbf{Q}_j$. Next, compute the second time derivative of the Lyapunov function, which results in

$$\ddot{V}(t) = \frac{2}{m_j}\boldsymbol{\phi}_j^{\mathrm{T}}\mathbf{D}_j^I\left[m_j\mathbf{S}(\boldsymbol{\omega}_j(t))\boldsymbol{\phi}_j + p_j\mathbf{S}^{-1}(\mathbf{M}_j) + \mathbf{D}_j^I\boldsymbol{\phi}_j\right].$$

Since the difference between matrices in SO(3) is bounded, then $\mathbf{M}_j$ is bounded. Moreover, recall that $\boldsymbol{\phi}_j$ is bounded and $\boldsymbol{\omega}_j$ is assumed to be bounded. Then, $\ddot{V}(t)$ is uniformly bounded, which implies that $\dot{V}(t)$ is uniformly continuous. Furthermore, since $V(t) \geqslant 0$ and $\dot{V}(t) \leqslant 0$, it follows that $V(t)$ converges to a limit, for any finite initial condition. Then, it follows from Barbalat's lemma that $\dot{V}(t)$ converges to zero (Khalil, 2002), which in turn implies that $\boldsymbol{\phi}_j$ converges to zero. If $\left(\mathbf{Q}_j^I(t), \mathbf{0}\right) \notin E_j$, then the error system evolves towards a state with $\boldsymbol{\phi}_j \neq 0$, because $\dot{\boldsymbol{\phi}}_j \neq 0$. Thus, $E_j = S_j \cup U_j$ is the largest forward invariant set.

Next, consider the linearization of the error dynamics about S_j. To that purpose, let $\mathbf{Q}_j^I \approx \mathbf{S}(\mathbf{x}) + \mathbf{I}$ and $\boldsymbol{\phi}_j \approx \mathbf{y}$, which yields

$$\begin{bmatrix}\dot{\mathbf{x}} \\ m_j\dot{\mathbf{y}}\end{bmatrix} = \begin{bmatrix}\mathbf{0} & \mathbf{R}_j^I \\ -2p_j(\hat{\mathbf{R}}_j^I)^{\mathrm{T}} & -m_j\mathbf{S}(\boldsymbol{\omega}_j) - \mathbf{D}_j\end{bmatrix}\begin{bmatrix}\mathbf{x} \\ \mathbf{y}\end{bmatrix}.$$

Similarly to the linearization about U_j, apply the transformation given by $\mathbf{z} = \frac{1}{\sqrt{2p_j}}\mathbf{R}_j^I\mathbf{y}$. It follows that

$$\begin{bmatrix}\dot{\mathbf{x}} \\ m_j\dot{\mathbf{z}}\end{bmatrix} = \begin{bmatrix}\mathbf{0} & \sqrt{2p_j}\mathbf{I} \\ -\sqrt{2p_j}\mathbf{I} & -(\hat{\mathbf{R}}_j^I)^{\mathrm{T}}\mathbf{D}_j(\hat{\mathbf{R}}_j^I)^{\mathrm{T}}\end{bmatrix}\begin{bmatrix}\mathbf{x} \\ \mathbf{z}\end{bmatrix}. \tag{23}$$

Let $\boldsymbol{\xi} = \begin{bmatrix}\mathbf{x} \\ \mathbf{z}\end{bmatrix}$ and $\mathbf{B} = \begin{bmatrix}\beta_1\mathbf{I} & \mathbf{0} \\ \mathbf{0} & \beta_2\mathbf{I}\end{bmatrix}$ and consider the Lyapunov candidate function

$$W(\boldsymbol{\xi}) = \frac{1}{2}\boldsymbol{\xi}^{\mathrm{T}}\mathbf{B}\boldsymbol{\xi}.$$

Therefore, its time derivative is given by $\dot{W}(t) = \beta_1 \mathbf{x}^{\mathrm{T}}\dot{\mathbf{x}} + \beta_2 \mathbf{z}^{\mathrm{T}}\dot{\mathbf{z}}$. Choose $\beta_1 = \beta_2 = \beta > 0$. Then, expanding the derivatives, using (23), recalling that $\mathbf{D}_j$ is positive definite, yields $\dot{W}(t) = -\boldsymbol{\xi}^{\mathrm{T}}\mathbf{C}^{\mathrm{T}}\mathbf{C}\boldsymbol{\xi} \leqslant 0$, where

$$\mathbf{C}(t) = \begin{bmatrix} \mathbf{0} & \mathbf{0} \\ \mathbf{0} & \sqrt{\beta}\mathbf{D}_j^{\frac{1}{2}}(\hat{\mathbf{R}}_j^I)^{\mathrm{T}} \end{bmatrix}. \tag{24}$$

Denote the linearized dynamics matrix in (23) by $\mathbf{A}_2$. Similarly to the argument in Khalil (2002, Example 8.11), if the pair $(\mathbf{A}_2, \mathbf{C})$ is uniformly completely observable (UCO), then $\mathbf{A}_2$ is globally exponentially stable and therefore the error system (13) is locally exponentially stable in $(\mathbf{I}, \mathbf{0})$. To show that the pair $(\mathbf{A}_2, \mathbf{C})$ is UCO, let

$$\mathscr{L}(t) = \begin{bmatrix} \mathbf{C}(t) \\ \mathbf{C}(t)\mathbf{A}_2(t) + \dot{\mathbf{C}}(t) \end{bmatrix},$$

where

$$\dot{\mathbf{C}}(t) = \begin{bmatrix} \mathbf{0} & \mathbf{0} \\ \mathbf{0} & \sqrt{\beta}\mathbf{D}_j^{\frac{1}{2}}\mathbf{S}(\boldsymbol{\omega}_j)^{\mathrm{T}}(\hat{\mathbf{R}}_j^I)^{\mathrm{T}} \end{bmatrix} \tag{25}$$

Thus, omitting the time dependence, it follows that

$$\begin{aligned}\mathscr{L}^{\mathrm{T}}\mathscr{L} = {} & \mathbf{C}^{\mathrm{T}}\mathbf{C} + \dot{\mathbf{C}}^{\mathrm{T}}\dot{\mathbf{C}} + \dot{\mathbf{C}}^{\mathrm{T}}\mathbf{C}\mathbf{A}_2 + (\mathbf{C}\mathbf{A}_2)^{\mathrm{T}}\dot{\mathbf{C}} \\ & + (\mathbf{C}\mathbf{A}_2)^{\mathrm{T}}\mathbf{C}\mathbf{A}_2.\end{aligned} \tag{26}$$

Denote (26) as the block matrix

$$\mathscr{L}^{\mathrm{T}}\mathscr{L} = \begin{bmatrix} \mathbf{L}_{11} & \mathbf{L}_{12} \\ \mathbf{L}_{12}^{\mathrm{T}} & \mathbf{L}_{22} \end{bmatrix}. \tag{27}$$

Then, from (23)-(25) and after some rearrangements, each block entry is respectively given as

$$\mathbf{L}_{11} = 2p_j\beta\mathbf{R}_j^I\mathbf{D}_j(\hat{\mathbf{R}}_j^I)^{\mathrm{T}},$$

$$\mathbf{L}_{12} = \beta\sqrt{2p_j}\mathbf{R}_j^I\mathbf{D}_j\mathbf{F}_j(\hat{\mathbf{R}}_j^I)^{\mathrm{T}},$$

and $\mathbf{L}_{22} = \beta\mathbf{R}_j^I\mathbf{D}_j\mathbf{R}_j^{I\mathrm{T}} + \beta\mathbf{R}_j^I\mathbf{F}_j^{\mathrm{T}}\mathbf{D}_j\mathbf{F}_j\mathbf{R}_j^{I\mathrm{T}}$,

where $\mathbf{F}_j = [\mathbf{S}(\boldsymbol{\omega}_j) + \mathbf{D}_j]$. Since $\mathbf{D}_j$ is positive definite, then $\mathbf{L}_{11}$ is positive definite. Moreover, the Schur complement with respect to $\mathbf{L}_{11}$, hereby denoted by $\mathscr{L}/\mathbf{L}_{11} = \mathbf{L}_{22} - \mathbf{L}_{12}^{\mathrm{T}}\mathbf{L}_{11}^{-1}\mathbf{L}_{12}$, which noticing that $\mathbf{L}_{11}^{-1} = \frac{1}{2p_j\beta}\mathbf{R}_j^I\mathbf{D}_j^{-1}\mathbf{R}_j^{I\mathrm{T}}$ and after some rearrangements yields

$$\begin{aligned}\mathscr{L}/\mathbf{L}_{11} = {} & \beta\mathbf{R}_j^I\mathbf{D}_j\mathbf{R}_j^{I\mathrm{T}} + \beta\mathbf{R}_j^I\mathbf{F}_j^{\mathrm{T}}\mathbf{D}_j\mathbf{F}_j\mathbf{R}_j^{I\mathrm{T}} \\ & -\beta\mathbf{R}_j^I\mathbf{F}_j^{\mathrm{T}}\mathbf{D}_j\mathbf{D}_j^{-1}\mathbf{D}_j\mathbf{F}_j\mathbf{R}_j^{I\mathrm{T}}.\end{aligned}$$

Then, $\mathscr{L}/\mathbf{L}_{11} = \beta\mathbf{R}_j^I\mathbf{D}_j\mathbf{R}_j^{I\mathrm{T}}$, which means that the Schur complement is positive definite as well. Therefore, (27) is positive definite and the pair $(\mathbf{A}_2, \mathbf{C})$ is UCO Bristeau et al. (2010, Theorem 4). This concludes the second part of the proof.

Finally, consider a point $(\mathbf{Q}_u, \boldsymbol{\phi}_u) \in U_j$, which, recalling (19), implies that the value of the Lyapunov function defined by (20) for any such point is $V(t) = 4p_j$. Moreover, any neighborhood of $(\mathbf{Q}_u, \boldsymbol{\phi}_u)$ includes states for which $V(t) < 4p_j$, for instance by varying $\mathbf{Q}_j$, while fixing $\boldsymbol{\phi}_u = \mathbf{0}$. Any trajectory with such initial conditions does not converge to U_j because $\dot{V}(t) \leqslant 0$ and therefore the set U_j is unstable relative to (13). There are, however, a set of specific trajectories that converge to U_j along the center stable manifold (Khalil, 2002). From classical center manifold theory, those trajectories are zero-measure in the overall space and since U_j is a zero-measure subset of $\mathrm{SO}(3) \times \mathbb{R}^3$, then the proof is complete.

4. Discrete-time observer

The observer implementation uses a discrete-time version of the observer derived in the previous section. This version is a Lie group variational integrator (LGVI) and assumes that the measurements are obtained at an appropriate constant rate in discrete-time. The stability properties are the same for both versions of the observer since LGVI maintain the properties of variational mechanics (Izadi and Sanyal, 2014).

Let the subscript k denote the k-th time instant in a set of N equally spaced sub-intervals, with time step denoted by Δt. The derivation of the discrete-time filter relies firstly on the discretization of the Lagrangian, which is given by

$$\mathscr{L}_{jk} = T_{jk} - U_{jk} = \frac{m_j}{2}\boldsymbol{\phi}_{jk}^{\mathrm{T}}\boldsymbol{\phi}_{jk} - p_j\mathrm{trace}\left(\mathbf{I} - \mathbf{Q}_{jk}^I\right).$$

Next, consider the discrete attitude kinematics given as

$$\dot{\hat{\mathbf{R}}}_{jk+1}^I = \hat{\mathbf{R}}_{jk}^I \exp\left[\Delta t\mathbf{S}(\hat{\boldsymbol{\omega}}_{jk})\right].$$

Then, the first variation of the discrete estimates for the attitude and angular velocity are respectively given by (Izadi and Sanyal, 2014)

$$\delta\hat{\mathbf{R}}_{jk}^I = \hat{\mathbf{R}}_{jk}^I\mathbf{S}(\eta_{jk})$$

and

$$\Delta t\delta\hat{\boldsymbol{\omega}}_{jk} = \eta_{jk+1} - \exp\left[-\Delta t\mathbf{S}(\hat{\boldsymbol{\omega}}_{jk})\right]\eta_{jk}.$$

Applying the discrete formulation of the Lagrange-d'Alembert principle (Marsden and West, 2001) to the sum of the discrete action functional and a discrete damping term results in

$$\delta s_{jk} + \Delta t\sum_{i=0}^{N-1}\tau_{\mathbf{D}_j k}^{\mathrm{T}}\eta_{jk} = 0,$$

Finally, considering the first variation of the discrete Lagrangian and the damping term $\tau_{\mathbf{D}_j k+1} = \mathbf{D}_j\boldsymbol{\omega}_{jk}$, the discrete-time version of the filter is expressed as

$$\dot{\hat{\mathbf{R}}}_{jk+1}^I = \hat{\mathbf{R}}_{jk}^I \exp\left[\Delta t\mathbf{S}(\hat{\boldsymbol{\omega}}_{jk})\right] \tag{28a}$$

and

$$m_j\dot{\boldsymbol{\phi}}_{jk+1} = \exp\left[-\Delta t\mathbf{S}(\hat{\boldsymbol{\omega}}_{jk})\right]\left[(m_j\mathbf{I} - \Delta t\mathbf{D}_j)\boldsymbol{\phi}_{jk} - \Delta tp_j\mathbf{S}^{-1}(\mathbf{M}_{jk+1})\right], \tag{28b}$$

with $\mathbf{M}_{jk+1} = \hat{\mathbf{R}}^{I\,T}_{jk+1}\mathbf{R}^{I}_{jk+1} - \mathbf{R}^{I\,T}_{jk+1}\hat{\mathbf{R}}^{I}_{jk+1}$, and $\hat{\boldsymbol{\omega}}_{jk} = \boldsymbol{\omega}_{jk} - \boldsymbol{\phi}_{jk}$. For further details about the derivation of these equations, see (Izadi and Sanyal, 2014).

5. Simulation

The performance of the proposed observer was assessed in the presence of sensor noise using a series of numerical simulations. First, a nominal configuration and maneuver were defined and implemented, considering the assumptions of the observer design. Then, a set of 1000 Monte Carlo simulations, whose initial conditions were perturbed relative to the nominal configuration, were implemented computationally to further assess the observer stability in a larger set of configurations.

Since each vehicle employs its own attitude observer, the nominal initial configuration is different for each vehicle, thus showing different aspects of the observer performance. Therefore, the initial attitude error for vehicle 1 starts close to the origin. The initial attitude error for vehicle 2 starts far from the origin, but still in the stable manifold S_2. Finally, the initial attitude error for vehicle 3 starts at the unstable manifold U_3.

This section starts with the description of the measurement and motion models. Then, the nominal initial configuration and maneuver are defined, followed by the description of the input perturbation models and respective parameters. Next, the simulation setup is defined and, finally, the results are given respectively for a single nominal simulation and for a set of perturbed configurations.

5.1. Measurement model

The line of sight and inertial reference measurements follow the model of the large field of view focal plane sensor (Cheng et al., 2006). In this model, the sensor gives two coordinates, $\mathbf{m} = [\chi, \psi]$, whose measurement is expressed as

$$\mathbf{m}_{\mathbf{m}} = \mathbf{m} + \mathbf{n}, \tag{29}$$

i.e. the sum of the true value with a zero mean random Gaussian noise, $\mathbf{n} \sim \mathcal{N}(\mathbf{0}, \mathbf{P}^F)$. The covariance in the focal plane is given by

$$\mathbf{P}^F = \frac{\sigma_d^2}{1 + (\chi^2 + \psi^2)} \begin{bmatrix} (1+\chi^2)^2 & (\chi\psi)^2 \\ (\chi\psi)^2 & (1+\psi^2)^2 \end{bmatrix},$$

where σ_d is the standard deviation of the focal coordinates. The transformation from the focal coordinates into the sensor frame unit vector is given as

$${}^{s}\mathbf{d} = \frac{1}{\sqrt{1+\chi^2+\psi^2}}[\chi, \psi, 1]^{\mathrm{T}},$$

where the focal length is assumed to be equal to one. The angular velocity measurement follows the discrete-time unbiased rate gyro model given by (Markley and Crassidis, 2014)

$$\boldsymbol{\omega}_{j_m} = \boldsymbol{\omega}_j + \sigma_{\omega_j}\Delta t^{-\frac{1}{2}}\mathbf{N}_j, \tag{30}$$

where $\boldsymbol{\omega}_{j_m}$ is the angular velocity measurement, σ_{ω_j} is the standard deviation of the noise, and $\mathbf{N}_j \sim \mathcal{N}(\mathbf{0}, \mathbf{I})$.

5.2. Motion model

The true values of the attitude follow the kinematics (2). Moreover, the model of the dynamics for a rigid body, which can represent spacecraft in flight, determines the ground truth of the angular velocity for each vehicle. Considering vehicle j, such model is given by

$$\dot{\boldsymbol{\omega}}_j = \mathbf{J}_j^{-1}\left(\boldsymbol{\tau}_{F_j} - \mathbf{S}(\boldsymbol{\omega}_j)\mathbf{J}_j\boldsymbol{\omega}_j\right), \tag{31}$$

where $\boldsymbol{\tau}_{F_j}$ represents an external moment applied to each vehicle given in $\mathrm{N\,m^{-1}}$, and $\mathbf{J}_j$ denotes the matrix of the moment of inertia given in $\mathrm{kg\,m^2}$.

5.3. Nominal initial conditions

The nominal initial configuration of the formation considers the inertial attitudes given by the identity matrix, i.e. $\mathbf{R}_1^I = \mathbf{R}_2^I = \mathbf{R}_3^I = \mathbf{I}$.

The inertial references are constant and given by

$${}^{I}\mathbf{d}_1 = \begin{bmatrix} 1 \\ 0 \\ 0 \end{bmatrix}, {}^{I}\mathbf{d}_2 = \begin{bmatrix} 0 \\ 1 \\ 0 \end{bmatrix}, \text{and } {}^{I}\mathbf{d}_3 = \begin{bmatrix} 0 \\ 1 \\ 0 \end{bmatrix},$$

whereas the inertial relative directions are initially given by

$${}^{I}\mathbf{d}_{1/2} = \mathbf{R}_1^I\mathbf{d}_{1/2} = \begin{bmatrix} 0 \\ \frac{1}{\sqrt{2}} \\ \frac{1}{\sqrt{2}} \end{bmatrix} \text{ and } {}^{I}\mathbf{d}_{1/3} = \mathbf{R}_1^I\mathbf{d}_{1/3} = \begin{bmatrix} 0 \\ 0 \\ 1 \end{bmatrix}.$$

Finally, the initial angular velocities are given, in rad/s, by $\boldsymbol{\omega}_1 = \boldsymbol{\omega}_2 = \boldsymbol{\omega}_3 = [0.1; 0.1; 0.1]^{\mathrm{T}}$.

5.4. Nominal maneuver

It is assumed that the vehicles can readjust their relative positions. The nominal maneuver affects only the relative position of vehicle 2. Thus, the value of ${}^{I}\mathbf{d}_2$ is given by the following update equation

$${}^{I}\mathbf{d}_{2k+1} = \mathbf{R}(\alpha_1, \mathbf{n}_1)\,{}^{I}\mathbf{d}_{2k} \tag{32}$$

with $\alpha_1 = \Delta t\frac{\pi}{240}$ and $\mathbf{n}_1 = \left[0 \; -\frac{1}{\sqrt{2}} \; \frac{1}{\sqrt{2}}\right]^{\mathrm{T}}$. The subscript k indicates the current time instant and Δt is the simulation time step.

This maneuver intentionally avoids the special cases of the formation described in (CCruz and Batistaruz and Batista, 2020), because these would result in a set with multiple solutions for the reconstructed attitudes driving the observers.

In the inertial frame, only the measurements of the relative direction between vehicles 1 and 2 vary, while all other measurements are constant in that frame. The nominal evolution of ${}^I\mathbf{d}_{1/2}$ is depicted in Fig. 2. Note that the orange and green lines are overlapped because the second and third elements of ${}^I\mathbf{d}_{1/2}$ have the same initial values and the maneuver maintains ${}^I\mathbf{d}_{1/2}$ in the plane where both elements are identical.

5.5. Perturbed initial configuration model

The Monte Carlo simulations consider a large set of trials where the initial configuration is perturbed in relation to the nominal initial conditions.

The initial values of ${}^I\mathbf{d}_1, {}^I\mathbf{d}_2, {}^I\mathbf{d}_3, {}^I\mathbf{d}_{1/2}$, and ${}^I\mathbf{d}_{1/3}$, which are three-dimensional unit vectors, are perturbed by a small rotation which changes their direction. Denote the unit vector of the nominal initial configuration as $\mathbf{n}_\mathbf{n}$. Then, the perturbed unit vector is given as

$$\mathbf{n} = \mathbf{R}\left(\delta\theta, \frac{\mathbf{S}(\mathbf{n}_\mathbf{n})\mathbf{r}}{\mathbf{S}(\mathbf{n}_\mathbf{n})\mathbf{r}}\right)\mathbf{n}_n, \tag{33}$$

with $\delta\theta \sim \mathcal{N}(\mathbf{0}, \sigma_\theta)$ and $\mathbf{r}$ denoting a random unit vector.

The initial values of $\boldsymbol{\omega}_1, \boldsymbol{\omega}_2$, and $\boldsymbol{\omega}_3$, which are three-dimensional vectors, are perturbed at two levels. Denote the vector of the nominal initial configuration as $\mathbf{v}_n$. Then, the perturbed vector is given by

$$\mathbf{v} = s\mathbf{R}\left(\delta\theta, \frac{\mathbf{S}(\mathbf{v}_\mathbf{n})\mathbf{r}}{\mathbf{S}(\mathbf{v}_\mathbf{n})\mathbf{r}}\right)\mathbf{v}_n, \tag{34}$$

with $\delta\theta \sim \mathcal{N}(\mathbf{0}, \sigma_\theta)$, $s \sim \mathcal{N}(\mathbf{0}, \sigma_s)$, and $\mathbf{r}$ denoting a random unit vector.

The initial values of $\mathbf{R}_1^I, \mathbf{R}_2^I$, and $\mathbf{R}_3^I$, which are rotation matrices, are perturbed at the level of the angle and axis. Denote the rotation angle of the nominal initial configuration as θ_n and the rotation axis of the nominal initial configuration as $\mathbf{n}_n$. Then, the perturbed rotation is given as

$$\mathbf{R} = \mathbf{R}\left(\theta_n + \delta\theta, \mathbf{R}\left(\delta\psi, \frac{\mathbf{S}(\mathbf{n}_n)\mathbf{r}}{\mathbf{S}(\mathbf{n}_n)\mathbf{r}}\right)\mathbf{n}_n\right), \tag{35}$$

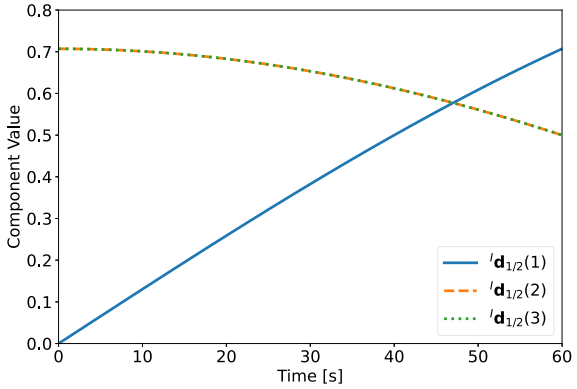

Fig. 2. Evolution of ${}^I\mathbf{d}_{1/2}$.

with $\delta\theta \sim \mathcal{N}(\mathbf{0}, \sigma_\theta)$, $\delta\psi \sim \mathcal{N}(\mathbf{0}, \sigma_\psi)$, and $\mathbf{r}$ denoting a random unit vector.

The perturbation parameters were chosen considering the observer assumptions. Thus, the angular velocities must be bounded and the degenerate attitude configurations must be avoided. The standard deviation values for each variable are given in Tables 1 and 2.

5.6. Simulation setup

For all trials, the vehicles are assumed identical and cylindrical. Therefore, the moment of inertia is a diagonal matrix with the entries respectively given by $\frac{m}{12}(3r^2 + h^2), \frac{m}{12}(3r^2 + h^2)$, and $\frac{m}{2}r^2$, where $m = 120$ kg, $h = 2$ m, and $r = 1$ m. Moreover, the external torque applied to each vehicle is a sinusoidal signal, where each component is given as

$$\boldsymbol{\tau}_F = 0.5\sin(f\Delta t)$$

in N.m, with $f = 1$ rad s^{-1}, which ensures that the angular velocity is bounded and thus satisfying all the assumptions, because its measurements were assumed unbiased. The true values of the components of $\boldsymbol{\omega}_1$, which are identical to the components of $\boldsymbol{\omega}_2$ and $\boldsymbol{\omega}_3$, are depicted in Fig. 3.

The ground truth of all measurements used in the attitude reconstruction must be defined for each time instant. Thus, it is assumed that the sensors have an appropriate sampling rate. For simplicity, the vision-based measurements are assumed to be taken by a focal plane sensor facing the body-fixed frame axes orthogonal to the highest component of the vector. The standard deviation of the several focal plane sensors is identical and given by $\sigma_d = 17 \times 10^{-6}$ rad, whereas the standard deviation of the rate gyros is $\sigma_{\omega_j} = 4.8 \times 10^{-6}$ rad/s.

The initial proximity of the errors to the origin is controlled by the initial estimates of the observer. Therefore, the initial attitude estimates are given, respectively, by

$$\hat{\mathbf{R}}_1^I(t_0) = \begin{bmatrix} 0 & 0 & -1 \\ 0 & 1 & 0 \\ 1 & 0 & 0 \end{bmatrix},$$

$$\hat{\mathbf{R}}_2^I(t_0) = \begin{bmatrix} \frac{1}{\sqrt{2}} & 0 & -\frac{1}{\sqrt{2}} \\ 0 & 1 & 0 \\ -\frac{1}{\sqrt{2}} & 0 & -\frac{1}{\sqrt{2}} \end{bmatrix},$$

and

Table 1
Perturbed initial attitude standard deviations.

	σ_θ [rad]	σ_ψ [rad]
$\mathbf{R}_1^I$	$\frac{\pi}{2}$	$\frac{\pi}{4}$
$\mathbf{R}_2^I$	$\frac{\pi}{2}$	$\frac{\pi}{4}$
$\mathbf{R}_3^I$	$\frac{\pi}{2}$	$\frac{\pi}{4}$

Table 2
Perturbed initial angular velocities standard deviations.

	σ_θ	σ_s
	[rad]	
$\boldsymbol{\omega}_1$	$\frac{\pi}{6}$	0.1
$\boldsymbol{\omega}_2$	$\frac{\pi}{6}$	0.1
$\boldsymbol{\omega}_3$	$\frac{\pi}{6}$	0.1

Table 3
Perturbed inertial measurements standard deviations.

	σ_θ [rad]
${}^I\mathbf{d}_1$	$\frac{\pi}{20}$
${}^I\mathbf{d}_2$	$\frac{\pi}{20}$
${}^I\mathbf{d}_3$	$\frac{\pi}{20}$
${}^I\mathbf{d}_{1/2}$	$\frac{\pi}{20}$
${}^I\mathbf{d}_{1/3}$	$\frac{\pi}{20}$

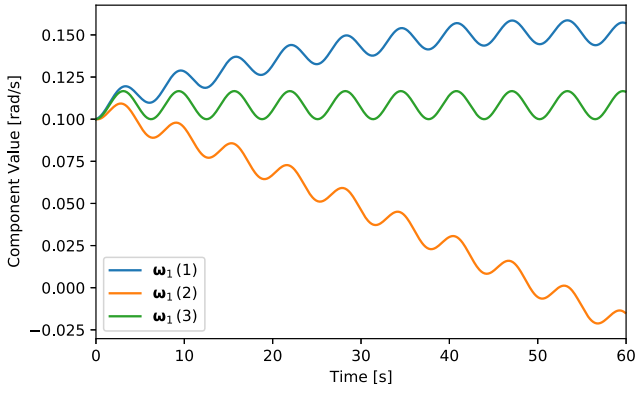

Fig. 3. Evolution of $\boldsymbol{\omega}_1$.

$$\hat{\mathbf{R}}_3^I(t_0) = \begin{bmatrix} 1 & 0 & 0 \\ 0 & -1 & 0 \\ 0 & 0 & -1 \end{bmatrix}.$$

The initial estimates of the angular velocities for $\hat{\boldsymbol{\omega}}_1$ and $\hat{\boldsymbol{\omega}}_2$are the zero vector, which means that the respective initial errors are $\boldsymbol{\phi}_1(t_0) = \boldsymbol{\omega}_1(t_0)$ and $\boldsymbol{\phi}_2(t_0) = \boldsymbol{\omega}_2(t_0)$. Since the third vehicle estimate is in manifold U_3, then $\boldsymbol{\phi}_3(t_0) = \mathbf{0}$, or equivalently $\hat{\boldsymbol{\omega}}_3(t_0) = \boldsymbol{\omega}_3(t_0)$. Moreover, the observer constant parameters are set to $m_j = 1.5, p_j = 1$, and $\mathbf{D}_j = \mathbf{I}$.

The simulation interval is 60 s with a time step of 0.1 s. In each iteration, the true values are updated according to (2), (31) and (32). Then, the vision sensor and rate gyro measurements are generated following the noise models described in (29) and (30). Next, from the vision-based measurements, the deterministic algorithm reconstructs each attitude in the formation. Finally, the attitude estimates are computed with (28), first the kinematics yield new attitude estimates and then the new feedback term is updated, by solving the respective equation numerically. After the simulation is complete, the attitude estimates are processed and the attitude errors, in matrix form, computed from (8). Then, the error matrices are transformed into the principal angle of the attitude error by

$$\boldsymbol{\epsilon}_j := \arccos\left(\frac{\text{trace}\left(\mathbf{Q}_j^I\right) - 1}{2}\right)$$

with $j = 1, 2, 3$ and the values of $\boldsymbol{\epsilon}_j$ in the interval $[0, \pi]$.

5.7. Monte Carlo setup

The Monte Carlo numerical implementation considers a set of 1000 trials, in which the initial configuration is perturbed according to (33)-(35), with the standard deviations presented in the Tables 1 and 2. Each trial follows the procedure given in the simulation setup description and the maneuver is always given by the update in (32).

5.8. Simulation results

Two sets of results are considered in this analysis: one with the nominal initial configuration results and another with the Monte Carlo trials results. The attitude errors are represented by their principle angle as an indication of their magnitude. Another error considered is the norm of the feedback parameter $\boldsymbol{\phi}_j$, which informs on the discrepancies of the angular velocity errors. The nominal initial configuration attitude errors, for all three vehicles, are given in Fig. 4, while the associated feedback parameters are given in Fig. 5. In the Monte Carlo experiment, both the reconstructed attitude error and the observer estimate error are considered. The respective results for all 1000 trials are condensed into their mean value relative to each time instant. The associated standard deviation is computed as well, which gives a more complete statistical representation. Both are depicted in Figs. 6–8, where the line represents the mean and the shaded area delimits the standard deviation from the mean of the respective instant of time.

The results for the nominal initial configuration, in Figs. 4 and 5, show that vehicle 3 converges to the correct

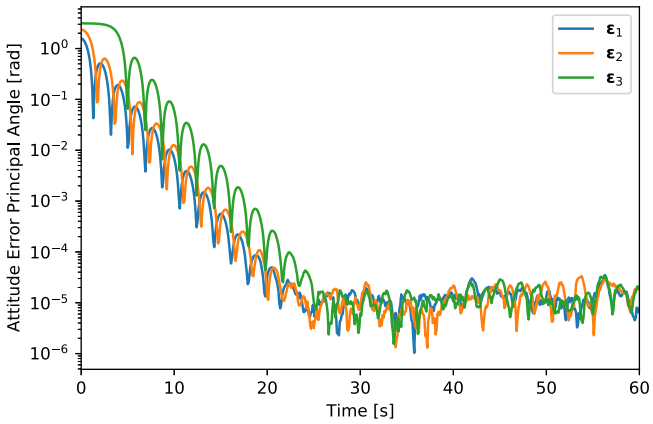

Fig. 4. Nominal simulation attitude errors.

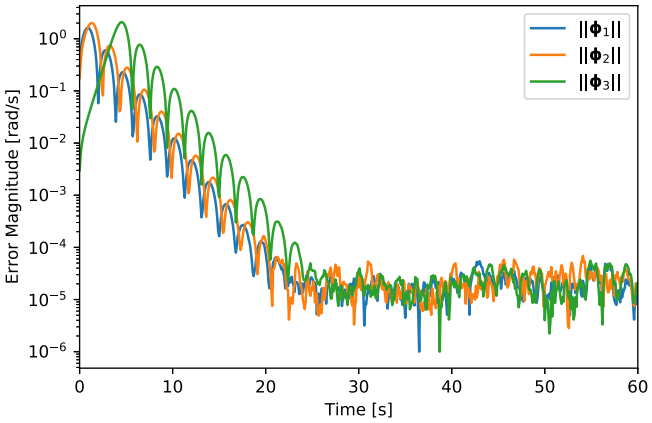

Fig. 5. Nominal simulation angular velocity errors.

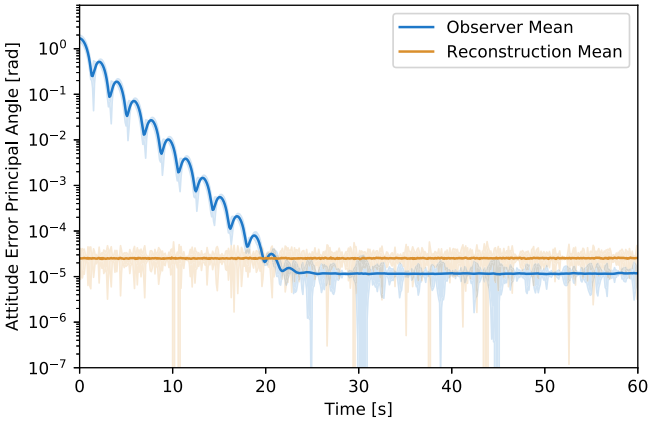

Fig. 6. Monte Carlo results for ϵ_1.

attitude, even though it is initially in the unstable equilibrium set U_3. Another possible observation, is that the feedback terms converge to a value within a given error of the zero vector due to sensor noise.

The results for the Monte Carlo trials, in Figs. 6–8, show that the observer errors tend to a smaller error than the error of the reconstructed attitude. Thus, the observer is using the rate gyro information to filter the reconstructed

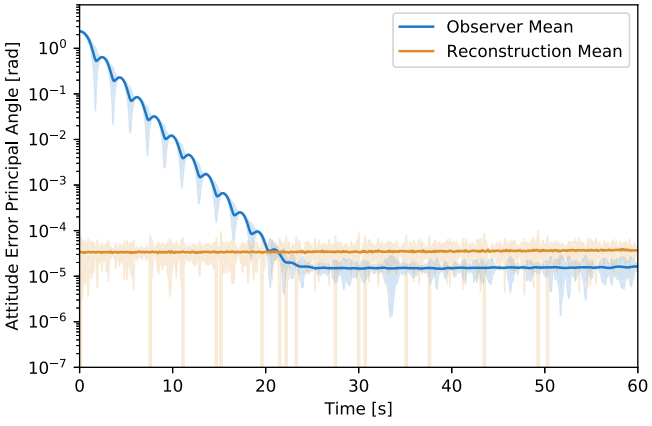

Fig. 7. Monte Carlo results for ϵ_2.

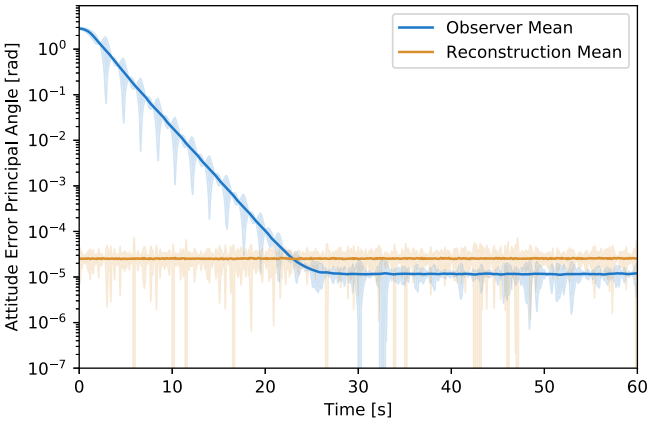

Fig. 8. Monte Carlo results for ϵ_3.

attitude errors and improve the accuracy of the estimation. Secondly, from the shaded areas, which are representing the standard deviation relative to the mean, the observer attitude errors do not vary significantly from the mean, despite the varying initial configuration of each trial. More importantly, the sum of the standard deviation and mean of the observer are lower than the analogous value of the reconstructed attitude, which reinforces the conclusions made regarding the respective mean values.

To summarize, if all assumptions are satisfied, that is the angular velocity is bounded and unbiased, while the reconstructed attitude exists and is unique, then the observer estimate errors converge to close to the origin. Moreover, these errors are smaller than the errors from the sensor attitude reconstruction, which indicate that the observer is filtering some of the noise of those sensors by using the rate gyros.

6. Conclusions

A reconstructed attitude was used to design an attitude observer, based on the Lagrange-d'Alembert principle of variational mechanics. The observer error is locally exponentially stable and converges to the origin for almost all initial conditions. The remaining equilibrium points are unstable and a zero measure subset of the domain. The observer was applied to the three-vehicle heterogeneous formations and tested using numerical simulations, where the performance of the solution with sensor noise was assessed. It was shown that the estimates in the unstable equilibrium manifold converge to the true attitude as well. Moreover, the numerical implementation showed that the observer errors are lower than the attitude reconstruction errors and thus the observer filters some of the errors in the attitude reconstruction. The application to the three vehicle heterogeneous formation is limited to cases where the attitude can be reconstructed unambiguously, because large errors in such variables result in the divergence of the results from the zero error estimates, because the observer is driven directly by the reconstructed attitude. This is

not a limitation of the observer. Instead, it is an intrinsic theoretical limitation of the problem framework, as discussed in (Cruz and Batista, 2020).

Declaration of Competing Interest

The authors declare that they have no known competing financial interests or personal relationships that could have appeared to influence the work reported in this paper.

Acknowledgment

The work of P. Cruz was supported by the PhD Grant PD/BD/143143/2019 from FCT. This work was also supported by the Fundação para a Ciência e a Tecnologia (FCT) through LARSyS - FCT Project UIDB/50009/2020 and through the FCT project DECENTER [LISBOA-01–0145-FEDER-029605], funded by the Programa Operacional Regional de Lisboa 2020 and PIDDAC programs.

References

Aguiar, A.P., Hespanha, J.P., 2006. Minimum-energy state estimation for systems with perspective outputs. IEEE Trans. Autom. Control 51 (2), 226–241. https://doi.org/10.1109/TAC.2005.861686.

Andrle, M.S., Crassidis, J.L., Linares, R., Cheng, Y., Hyun, B., 2009. Deterministic relative attitude determination of three-vehicle formations. J. Guid., Control, Dynam. 32 (4), 1077–1088. https://doi.org/10.2514/1.42849.

Batista, P., Silvestre, C., Oliveira, P., 2012. Globally exponentially stable cascade observers for attitude estimation. Control Eng. Pract. 20 (2), 148–155. https://doi.org/10.1016/j.conengprac.2011.10.005.

Black, H., 1964. A passive system for determining the attitude of a satellite. AIAA J. 2 (7), 1350–1351. https://doi.org/10.2514/3.2555.

Bristeau, P., Petit, N., Praly, L., 2010. Design of a navigation filter by analysis of local observability. In: In 49th IEEE Conference on Decision and Control (CDC), pp. 1298–1305. https://doi.org/10.1109/CDC.2010.5717848.

Cao, Y., Fukunaga, A., Kahng, A., 1997. Cooperative mobile robotics: Antecedents and directions. Autonomous Robots 4, 7–27. https://doi.org/10.1023/A:1008855018923.

Cesarone, R., Abraham, D., Deutsch, L., 2007. Prospects for a next-generation deep-space network. Proc. IEEE 95, 1902–1915. https://doi.org/10.1109/JPROC.2007.905043.

Cheng, Y., Crassidis, J.L., Markley, F.L., 2006. Attitude estimation for large field-of-view sensors. Journal of the Astronautical Sciences 54 (3), 433–448. https://doi.org/10.1007/BF03256499.

Crassidis, J.L., Markley, F.L., Cheng, Y., 2007. Survey of nonlinear attitude estimation methods. Journal of Guidance, Control, and Dynamics 30 (1), 12–28. https://doi.org/10.2514/1.22452.

Cruz, P., Batista, P., 2019. A solution for the attitude determination of three-vehicle heterogeneous formations. Aerosp. Sci. Technol. 93, 105275. https://doi.org/10.1016/j.ast.2019.07.008.

Cruz, P., & Batista, P. (2020). Special cases in the attitude determination of three-vehicle heterogeneous formations. In 2020 7th International Conference on Control, Decision and Information Technologies (CoDIT) (pp. 136–141). volume 1. doi:10.1109/CoDIT49905.2020.9263956.

Cruz, P., Batista, P., & Sanyal, A. (2021). Attitude observers for three-vehicle heterogeneous formations based on the lagrange-d'alembert principle. In European Control Conference.

Izadi, M., Sanyal, A.K., 2014. Rigid body attitude estimation based on the lagrange-d'alembert principle. Automatica 50 (10), 2570–2577. https://doi.org/10.1016/j.automatica.2014.08.010.

Khalil, H., 2002. Nonlinear Systems. Pearson Education, (3rd ed.). Prentice Hall.

Kim, S.-G., Crassidis, J.L., Cheng, Y., Fosbury, A.M., & Junkins, J.L. (2007). Kalman Filtering for Relative Spacecraft Attitude and Position Estimation. Journal of Guidance, Control, and Dynamics, 30(1), 133–143. URL: doi: 10.2514/1.22377. doi:10.2514/1.22377. Publisher: American Institute of Aeronautics and Astronautics _eprint: https://doi.org/10.2514/1.22377.

Li, X., Sanyal, A.K., Warier, R.R., Qiao, D., 2020. Landing of hopping rovers on Irregularly-shaped small bodies using attitude control. Adv. Space Res. 65 (11), 2674–2691. https://doi.org/10.1016/j.asr.2020.02.029.

Linares, R., Crassidis, J.L., Cheng, Y., 2011. Constrained relative attitude determination for two-vehicle formations. Journal of Guidance, Control and Dynamics 34 (2), 543–553. https://doi.org/10.2514/1.50053.

Mahony, R., Hamel, T., Pflimlin, J., 2008. Nonlinear complementary filters on the special orthogonal group. IEEE Trans. Autom. Control 53 (5), 1203–1218. https://doi.org/10.1109/TAC.2008.923738.

Markley, F.L., Crassidis, J.L., 2014. Fundamentals of Spacecraft Attitude Determination and Control, 1st ed. Microcosm Press and Springer, New York.

Marsden, J.E., West, M., 2001. Discrete mechanics and variational integrators. Acta Numerica 10, 357–514. https://doi.org/10.1017/S096249290100006X.

Misra, G., Izadi, M., Sanyal, A., Scheeres, D., 2016. Coupled orbit–attitude dynamics and relative state estimation of spacecraft near small Solar System bodies. Adv. Space Res. 57 (8), 1747–1761. https://doi.org/10.1016/j.asr.2015.05.023.

Sanyal, A.K., Lee, T., Leok, M., McClamroch, N.H., 2008. Global optimal attitude estimation using uncertainty ellipsoids. Systems & Control Letters 57 (3), 236–245. https://doi.org/10.1016/j.sysconle.2007.08.014.

Scharf, D.P., Hadaegh, F.Y., & Ploen, S.R. (2003). A survey of spacecraft formation flying guidance and control (part 1): guidance. In Proceedings of the 2003 American Control Conference, 2003. (pp. 1733–1739). volume 2. doi:10.1109/ACC.2003.1239845.

Wahba, G., 1965. A least squares estimate of satellite attitude. SIAM Review 7 (3), 409. https://doi.org/10.1137/1007077.

Wang, J., Zhang, R., Yuan, J., Luo, J., 2019. Multi-CubeSat Relative Position and Attitude Determination Based on Array Signal Detection in Formation Flying. IEEE Trans. Aerosp. Electron. Syst. 55 (6), 3378–3393. https://doi.org/10.1109/TAES.2019.2910362, URL: https://ieeexplore.ieee.org/document/8693887/.

Wu, J., 2020. Unified Attitude Determination Problem From Vector Observations and Hand-Eye Measurements. IEEE Trans. Aerosp. Electron. Syst. 56 (5), 3941–3957. https://doi.org/10.1109/TAES.2020.2982482, URL: https://ieeexplore.ieee.org/document/9044310/.

Wu, J., Zhou, Z., Gao, B., Li, R., Cheng, Y., Fourati, H., 2018. Fast Linear Quaternion Attitude Estimator Using Vector Observations. IEEE Trans. Autom. Sci. Eng. 15 (1), 307–319. https://doi.org/10.1109/TASE.2017.2699221.

Zamani, M., Trumpf, J., Mahony, R., 2011. Near-optimal deterministic filtering on the rotation group. IEEE Trans. Autom. Control 56 (6), 1411–1414. https://doi.org/10.1109/TAC.2011.2109436.